Nonlinear signalling networks and cell-to-cell variability transform external signals into broadly distributed or bimodal responses

Maciej Dobrzyński[1,*], Lan K. Nguyen[1], Marc R. Birtwistle[1,2], Alexander von Kriegsheim[1], Alfonso Blanco-Fernández[3], Alex Cheong[1,4], Walter Kolch[1,5,6], Boris N. Kholodenko[1,5,6,†]

1 Systems Biology Ireland, University College Dublin, Belfield, Dublin 4, Ireland

2 Icahn School of Medicine at Mount Sinai, One Gustave L. Levy Place, Box 1603, New York, NY 10029, USA

3 Flow Cytometry Core Technologies, Conway Institute of Biomolecular and Biomedical Research, University College Dublin, Belfield, Dublin 4, Ireland

4 School of Life and Health Sciences, Aston University, Birmingham B4 7ET, UK

5 Conway Institute of Biomolecular and Biomedical Research, University College Dublin, Belfield, Dublin 4, Ireland

6 School of Medicine and Medical Science, University College Dublin, Belfield, Dublin 4, Ireland

∗ **E-mail: maciej.dobrzynski@ucd.ie**

† **E-mail: boris.kholodenko@ucd.ie**

Abstract

We show theoretically and experimentally a mechanism behind the emergence of wide or bimodal protein distributions in biochemical networks with nonlinear input-output characteristics (the dose-response curve) and variability in protein abundance. Large cell-to-cell variation in the nonlinear dose-response characteristics can be beneficial to facilitate two distinct groups of response levels as opposed to a graded response. Under the circumstances that we quantify mathematically, the two distinct responses can co-exist within cellular population, leading to the emergence of a bimodal protein distribution. Using flow cytometry, we demonstrate the appearance of wide distributions in the Hypoxia-inducible Factor (HIF) mediated response network in HCT116 cells. With help of our theoretical framework we perform a novel calculation of the magnitude of cell-to-cell heterogeneity in the dose-response obtained experimentally.

Keywords: bimodality, cell heterogeneity, dose-response, signalling networks

Introduction

Thermal fluctuations inherently affect all biochemical reactions, and the variability in molecular copy numbers due to stochastic effects decreases, as the mean number of molecules in the system rises. Gene expression is inevitably stochastic, as usually there are not more than two gene copies in a cell. It is because of this biochemical noise that cells within an isogenic population, be it a bacterial colony or mammalian cells, at any given point in time exhibit a distribution of measurable properties rather than a precise value. Cells in genetically identical populations vary in, for example, size, the concentrations of proteins and mRNA, and the stage of progression along the cell cycle.

Quantification of biochemical noise requires single-cell techniques [1–5] capable of reconstructing the whole histogram (a distribution) of molecule counts over the entire cellular population. A bimodal (a double-peaked) distribution, is particularly interesting from the physiological point of view, as it indicates existence of two subpopulations with (possibly) distinct phenotypic features. For instance, a bimodal distribution of antibiotic-resistance protein, ZeoR, was suggested to increase viability of the yeast population treated with large doses of Zeocin [6]. In another study, heterogeneous response to treatment with a chemoterapeutic drug, camptothecin, resulted in a bimodal distribution of 24 protein accumulation slopes. Additionally, for the RNA helicase DDX5 and the replication factor RFC1 peaks of their bimodal distributions correlated with different cell fates: fast protein accumulation was found in cells that survived the treatment, while slow accumulation existed in cells undergoing changes associated with cell death [7, 8].

In biological systems bimodal distributions of protein concentrations at the population level can be generated by several mechanisms (Fig. 1). A genetic switch is the simplest mechanism. For a large difference between the rate of gene on/off switching and the turnover of the gene product, e.g. mRNA [9, 10], two distinct peaks of product abundance arise (Fig. 1A). Such infrequent gene expression bursts leading to bimodality have been observed in *E.coli* [11], yeast [12] and mammalian cells [2].

In the context of signalling networks, bistability is a well-known mechanism that can generate bimodal responses. It usually requires positive feedback that may be hidden or explicit (Fig. 1B) [13–16] or double negative feedback, as in synthetic toggle switch [17]. While stochastic switching requires nondeterministic

analysis in order to show the existence of two states, bistable systems can be analysed deterministically with classical ODEs. Importantly, bistability in the deterministic setting does not necessarily lead to bimodal distributions. Dynamic switching between two stable states has to be promoted by fluctuating biochemical reactions or by external noise [18], or by cell-to-cell variability in the thresholds for switching between two steady states [19, 20].

A much less appreciated mechanism capable of generating population-level bimodality relies on independently oscillating cells [21]. Cell-to-cell variability in protein abundances affects period and (or) phase of cells' oscillations which in turn generates a bimodal protein distribution (Fig. 1C). The existence of this distribution depends on the extent to which phases of oscillations vary between the cells (*phase mixing*) as well as functional form of oscillations, e.g. pure triangle wave will fail to generate bimodality. Notably, if cells oscillate with slightly variable period, the emergence of a bimodal distribution is inevitable with time.

The nature of mechanism leading to bimodality that we discuss here differs from that of stochastic switching, bistability or superposition of oscillations. Here, two distinctive peaks in steady-state distributions of protein concentrations that arise on the population level stem from the interplay of two factors: (i) nonlinear input-output characteristic (the response) of the biochemical network at the single-cell level [22,23], and (ii) cell-to-cell variability in the abundance of network components which translates to different input-output characteristics of that network across the population (Fig. 1D).

In the following sections we investigate analytically and numerically how bimodal steady-state protein distributions can emerge in nonlinear biochemical networks. We explore the effect of heterogeneity in the input signals (extrinsic noise) and/or variability in the input-output relationship due to stochastically expressed network components (intrinsic noise) on the population-level distributions of protein concentrations. We apply our theoretical framework to infer variability in dose responses across the cellular population from flow-cytometric measurements in the hypoxia response signalling system. We use a mathematical model of this system to demonstrate possible contributions to variability of the dose-response.

Results

Variability of response thresholds

The dose-response characteristics is a relationship between the magnitude of the input stimulus (e.g. growth factor concentration) and the output target, which can be the concentration of an active kinase (such as doubly-phosphorylated MAPK) or a transcription factor. It is a function that depends both on the concentration of network components and kinetic parameters of biochemical reactions that involve these components. This input-output relationship, $R(x)$, is commonly approximated by a Hill curve parameterised by four coefficients (β, x_{50}, R_{max}, H):

$$y = R(x, x_{50}, \beta, R_{max}, H) = \beta + R_{max}\frac{x^H}{x_{50}^H + x^H} \tag{1}$$

where x is the input signal (e.g. concentration of a drug or a toxin), β is basal response level, R_{max} is the maximum output level, and H is the Hill coefficient that determines the steepness of the response. The parameter x_{50} is the response threshold, also known as the half maximal effective concentration (EC_{50}). It is the concentration of the stimulus (the input x) for which the response assumes half of the maximum output (minus basal level)

We assume that cells within a population experience the same level of stimulation x. This condition holds during our experiments when cells are grown in a monolayer in a tissue culture and are subject to equal levels of treatment (input). What sets cells apart is the threshold x_{50} of the response function R. Such variability may stem from differences in the molecule numbers of the same network components and fluctuations in their activation levels. In mathematical terms, we describe this variability by the probability density function (*pdf*) of thresholds, $f_{x50}(x_{50})$. The resulting distribution of output y for a given input value x in the presence of variable thresholds x_{50} of the response function R is given by a general expression (Supplementary Equations 1-3),

$$f_{out}(y) = -f_{x50}(r_{x50}(y)) \cdot \frac{d}{dy} r_{x50}(y) \tag{2}$$

where $r_{x50}(y)$ is the inverse of the response function calculated with respect to threshold x_{50}. Note the "-" sign, which reflects the fact that the response function is monotonically decreasing with x_{50}.

Existence of bimodality

Intuitive conditions for the existence of bimodality can be obtained for a model system with Hill-type response function and log-normally distributed threshold x_{50} across the population. It can be demonstrated numerically that such a parameter distribution is indeed a reasonable approximation for signalling cascades with concentrations of network components log-normally distributed across the cellular population (Supplementary Figure S4). The assumption behind the distribution of protein concentrations is justified in the light of experimental evidence. Measurements have shown that protein distributions are log-normal around the mean with additional power-law tails that may arise from feedbacks in biochemical networks [24–26].

The first condition, necessary but not sufficient, relates the steepness H of the dose response with the shape parameter σ_{x50} of the log-normal distribution of x_{50} (Supplementary Equation 5),

$$H \cdot \sigma_{x50} > \sqrt{2} \tag{3}$$

where σ_{x50} is related to the squared coefficient of variation of x_{50} distribution, CV^2_{x50}, through: $\sigma_{x50} = \sqrt{\log\left(CV^2_{x50}+1\right)}$. Thus, steep (large H) steady-state response function R prompts a bimodal distribution even for very narrowly distributed thresholds (small σ_{x50}). And vice versa; bimodality may result from very heterogeneous but graded (small H) response function R.

Once H and σ_{x50} satisfy equation (3), a bimodal output distribution may arise but only when the input stimulus, x, is within the steep region of the mean response curve. Parameters H and σ_{x50} determine the width of that range. Bimodality will therefore ensue as long as the ratio of the input to the median of the threshold distribution, m_{x50}, satisfies:

$$\alpha^-(H,\sigma_{x50}) < \log\frac{x}{m_{x50}} < \alpha^+(H,\sigma_{x50}) \tag{4}$$

where $\alpha^{\mp}(H,\sigma_{x50})$ depends only on H and σ_{x50} (Supplementary Equation 15). The range of admissible x/m_{x50} ratios widens for a steep dose response and (or) large threshold variability (Supplementary Figure S2).

Hill function is only linearly dependent on β and R_{max}, hence variability in neither of these parameters alone can generate a bimodal output distribution (Fig. 2B). Variability in H can also introduce

bimodality, however, for inputs around the mid-point of the dose-response the distribution reverts to unimodal (Fig. 2C). Since protein distributions for a range of input stimuli that we observe experimentally correspond to those shown in figure 2A, we assume that variability in response threshold x_{50} contributes the most to the population-level protein variability.

Variability in the input stimulus x is mathematically equivalent to variability in x_{50}, therefore it is equally capable of generating bimodal distributions as has been argued previously in the context of transcriptional regulation [27–30]. In those scenarios, variable input signal corresponds to noisy concentration of a regulatory protein, e.g. a transcription factor. By fixing threshold x_{50} in equation (1) and by treating x as a variable subject to fluctuations described by a log-normal distribution, we obtain conceptually similar results as previously. The first condition is the same as previously stated in equation (3) with only difference that σ relates to variability of the input stimulus rather than the threshold. The interpretation of the second condition changes accordingly. Function $\alpha^{\mp}(H, \sigma_x)$ bounds the ratio of the input distribution's median m and now fixed threshold level x_{50}.

Equations (3) and (4) that warrant bimodal system response are derived for a specific case of a log-normal input or response threshold distribution and a Hill-type dose response. However, the interpretation of the two conditions holds also for other types of distributions and responses, e.g. gamma distribution, sigmoidal and logistic response characteristics. Equation (3) simply states that in order to facilitate a bimodal distribution both the steepness of the response and variability of thresholds must be coupled; reduction of the former requires an increase in the latter and vice versa. Equation (4) prescribes how far the mid-point of the threshold distribution (its "centre of mass") can be from the mid-point of the response (the steepest point) in order to maintain bimodality. These two conditions hold for other cases as well, although their exact mathematical form is not as simple as for log-normal distribution and Hill-type response. Notably, bimodality may arise only for nonlinear response characteristics. A linear dose response would result in a trivial result where the output distribution is simply a rescaled distribution of a given parameter in that response function.

Additionally, in order to generate bimodality, the dose-response cannot equal the cumulative distribution (CDF) of the variable parameter or, equivalently, the distribution cannot be a derivative of the response function [31]. If this is the case, the output distribution becomes uniform on the interval between the lowest and highest response. Consider a cell population with the response function $R(x;\, x_{50},\, H) = x^H/(x_{50}^H + x^H)$ and the threshold distribution across the ensemble $f_{x50}(x_{50};\, x,\, H)$ equal

to the derivative of R with respect to x_{50} (with a minus sign). Since f_{x50} depends also on the input stimulus x, the population-level response to any input value is a uniform distribution between 0 and 1. It implies that any signal evokes the exact same population-level response. However, from the biological perspective the scenario in which the dose-response always remains equal to the CDF of the threshold distribution is intriguing, yet unlikely. It requires x_{50} distribution to change with x, which in turn would affect the dose-response curve. In a more plausible scenario the system adapts its dose-response to the distribution of inputs that it experiences. It has been shown that a number of neural systems employ the strategy of matching the dose-response to CDF of inputs in the environment [31, 32] to fully utilise neurone's limited response range and maximise the information transfer: the most frequently perceived stimuli evoke outputs from the steepest region of the dose-response. Arguably, cellular signalling networks as discussed throughout this paper undergo this type of adaptation.

According to equation (4) the range of input/median ratios for which bimodality arises depends on the width of the threshold distribution, $\sigma_{x50} = \sqrt{\log\left(CV_{x50}^2 + 1\right)}$ (Supplementary Figure S2). The larger it is, the stronger becomes the separation of the heterogenous population into two groups with distinct levels of protein concentrations. Figure 3A-C depicts this intriguing property that runs counter to the conventional assumption that cellular variability destroys robust signalling. Here, we consider a system with a mildly ultrasensitive, $H = 3$, dose response. Compare this to $H \approx 5$ reported for the MAPK cascade [22], $H = 5 \ldots 9$ observed for Rap-GTP responding to Cannabinoid-1 receptor signal [33], or $H = 1 \ldots 4$ measured for a synthetic system with multiple autoinhibitory modules [34]. For $CV_{x50}^2 > 0.4$, protein distributions become significantly wider for input stimuli in the steepest part of the dose response. For $CV_{x50}^2 = 4$, the responses tend to concentrate around basal and saturation values and two peaks emerge for intermediate stimuli. Such bimodality may facilitate further decision-making, which is not entirely random but is performed based on two well-defined options instead.

Uncertainty of a distribution is often quantified by Shannon entropy [35]. Its low value indicates that small amount of information is required to describe the varying quantity, e.g. protein concentration across the population. Therefore, a peaked unimodal distribution requires a twice shorter description than a bimodal distribution with two narrow peaks. Any wide distribution in between requires more information than either of the two, which is reflected by high value of entropy. Figure 3D quantifies distributions induced by inputs equal to x_{50} of the dose-response (red dots in Fig. 3A-C). The entropy peaks at $CV_{x50}^2 \approx 2$ and decreases due to uncertainty introduced by threshold variability. However, for biologically

realistic values of CV^2_{x50} between 0.4 and 4 the distributions change their shape from wide to bimodal, while their entropy changes only slightly. This suggests that the quantification of uncertainty using entropy may be misleading as even protein distributions with large entropy may reveal a physiologically relevant widening of a population into two groups. Even though this division is not complete and a number of responses still appear between the peaks, such distributions have been demonstrated to be physiologically advantageous to the population [6].

Variability in hypoxia response network

In this section we study experimentally the cellular hypoxia response network, analyse the emergence of wide protein distributions and estimate the response variability from experimental data. When cellular oxygen demand exceeds supply, the cells enter a phase of hypoxia. As a consequence, stabilisation of the hypoxia-inducible factor (HIF) ensues. Stabilised HIF mediates transcription of genes to adapt to the hypoxic insult [36]. Central to the response is the action of prolyl-hydroxylases (PHD), enzymes that hydroxylate HIF at residues Pro-402 and Pro-564 [37] and target it for ubiquitination-degradation via the von Hippel-Landau protein (VHL) [38]. Figure 4 depicts a simplified scheme of the network.

For our experimental setup, we used a stable HCT116 cell line expressing a fragment of the HIF protein containing residues 403-603, termed the oxygen-dependent degradation (ODD) domain [39] tagged to GFP (cells courtesy of Prof. E. Gottlieb, [40]). The ODD-GFP is our readout of hypoxic response. We activate the system using the hydroxylase inhibitor dimethyloxalylglycine (DMOG), which mimics the condition of low oxygen level in the HIF system [41]. Cells in tissue culture were grown up to 70% confluency at the end of the treatment, which minimised the effect of cell contact and maintained cells in a monolayer such that all of them were exposed to equal levels of DMOG. Hence, any variability in the response can be attributed to intrinsic variations of network components in individual cells, which facilitates our aim of measuring dose-response variability while assuming fixed input. The condition, however, may not hold in general, especially when cells are embedded in tissue and/or subject to different micro-environments.

HIF responses to DMOG averaged over cell population

Using flow-cytometry we first identify a sigmoidal dose response. For each DMOG condition, we calculate the median of the single-cell ODD-GFP fluorescence across a population of minimum 10000 cells. In doing so, we derive the dose-response curve, i.e. the ODD-GFP response to DMOG. We normalise the median to

control, unstimulated case. The median response averaged over minimum 3 biological repeats at 4, 8 and $16h$ following DMOG addition is shown in figure 5A where we also fit the Hill model from equation (1) (Supplementary Table S1). The increase with time of the steepness, H, and the maximum response, R_{max}, is consistent with earlier measurements using Western blots [42], which supports the qualitative correspondence between population-averaged flow-cytometric and bulk measurements.

HIF response distributions across the cell population

Distributions of ODD-GFP fluorescence intensity (Fig. 5B) increase their width for DMOG = 1 and $2mM$. At these DMOG concentrations the response curve is the steepest; it is the most sensitive region of the cellular response. Widening of the ODD-GFP distribution for DMOG concentrations that induce the steepest region of the dose response hints at the existence of cell-to-cell variability in response thresholds (cf. Fig. 2). If there were no threshold variability, cells treated with DMOG would exhibit a peak of ODD-GFP distribution shifting towards higher values without increase in its width as shown in figure 3A. This is not what we observe experimentally. In the presence of threshold variability and steep nonlinear response, the distribution may widen or even become "split" between the low and high response – the fact quantified by equations (3) and (4), and illustrated by figure 3B-C. Consistently with our predictions, the observed widening of the ODD-GFP distribution becomes more pronounced the steeper the dose response and the larger the maximum response level. This is the case at 8h and $16h$ post-treatment.

As a next step, we estimate distributions of parameters β, R_{max} and x_{50} in the Hill model, equation (1), from a single experiment. Parameter H is assumed to be constant across the population and we calculate it by fitting the Hill curve to population-averaged dose responses (Supplementary Figure S5A and Supplementary Table S2). The distribution of basal level β is obtained from the ODD-GFP distribution measured for the unstimulated case, DMOG = $0mM$ (Supplementary Figure S5B and Supplementary Table S3). Based on our fits of the Hill function to the dose-response, we recognise that even at DMOG = $4mM$ the curve does not saturate. However, the ODD-GFP distribution at 8 and 16h post-DMOG treatment becomes left-skewed, which indicates that the system is not far from saturation. Since higher DMOG levels would be toxic to cells, we decide to use the response at DMOG = $4mM$ as a proxy of R_{max} variability. At that DMOG level, the response is also affected by an independent contribution from variability in the basal level β. We therefore subtract the mean and variance of β from the distribution due to DMOG = $4mM$ and use this new distribution as an estimate of R_{max} variability

(Supplementary Figure S5C and Supplementary Table S4).

Finally, we estimate variability in threshold x_{50}. At a given time point, for every DMOG concentration we record the value of ODD-GFP distribution at a half-distance between the mode (the peak) of the basal (DMOG $= 0\,mM$) and the maximum (DMOG $= 4\,mM$) distribution. Such a curve, which is a function of DMOG level, is largely independent of β, R_{max} and H, and is determined only by parameters of x_{50} distribution. The independence is exact when x_{50} is distributed log-normally (Supplementary Equation 17). After normalisation to 1, the function has the interpretation of the probability density, which can be used to determine parameters of the x_{50} distribution (Supplementary Figure S3, S5D and Supplementary Table S5).

For spread of parameters β and R_{max} across cell population, we fit gamma, log-normal and Weibull distributions. Based on Akaike information criterion (AIC) [43], we conclude that Weibull distribution is the best approximation of experimentally measured variability in both parameters (Supplementary Figures 5B & C and Tables S3 & S4). By applying these distributions to equation (1) we numerically calculate ODD-GFP distributions shown in figure 5C. Figure 5D quantifies the agreement between experimental and predicted ODD-GFP distributions with a dimensionless robust coefficient of variation, rCV, expressed by equation (6) in Materials and Methods.

According to our model, wide distributions that we observe experimentally can arise only in the presence of variability in response threshold, x_{50} (Fig. 2). We find that the dimensionless squared coefficient of variation (CV^2 = variance over squared mean) of fitted x_{50} distribution decreases from 2.72 at 4h, through 1.38 at 8h, down to 0.26 at 16h post-treatment. The decrease in CV^2_{x50} over time is compensated by increasing H, which promotes widening of the ODD-GFP distribution at DMOG concentrations that induce the steep part of the response. Substituting H and CV^2_{x50} into equation (3) reveals that the system remains in the same regime where only mild bimodality may arise (Supplementary Table S6 and Supplementary Figure S6). The distribution is further affected by variability in β and R_{max}, which results in widening instead of the emergence of two clearly separated peaks. The widening is reflected by the increase in rCV (Fig. 5D). In case of small x_{50} variability, or lack thereof, an increasing stimulus would induce a proportionally shifting peak of ODD-GFP distribution without widening as illustrated in figure 3A and quantified by a theoretical dotted line in figure 5D.

Response variability in mathematical model of HIF system

We employed a published mathematical model of the HIF system [42] to search for possible molecular sources causing large dose-response variability. First, we calculate numerically the response of the system at $16h$ to various oxygen tension levels, which affects HIF level in the opposite manner to DMOG treatment. The untreated case corresponds to 21% of oxygen, i.e. normoxia, while high DMOG treatment corresponds to hypoxic condition of low oxygen level. Hill function is then fitted to the calculated dose-response. In order to account for cell-to-cell heterogeneity we repeat this procedure 1000 times with total levels of all protein species drawn from a log-normal distribution with $CV^2 = 0.5$ and means fixed to the original ODE model (Supplementary Material of [42]). The chosen CV^2 is at the upper limit of measured protein variability in mammalian cells which typically ranges between 0.1 and 0.5 [7, 26, 44–46].

The mean and variability of the dose-response obtained from a population of deterministic models are shown in figure 6A. By fitting Hill function to each of the responses from the entire population we obtain distributions of parameters x_{50}, β, R_{max}, and H at $16h$ post-treatment (Figs. 6C-F). The distribution of H has the smallest CV^2 of all parameters, which justifies our choice of neglecting variability in H when estimating variability of Hill parameters from experimental data in previous section. The distribution of x_{50} is well approximated by a log-normal distribution and $CV^2_{x50} = 0.30$ is comparable with 0.26 that we estimated from experimental data in figure 5C. Additionally we perform local sensitivity analysis by randomly sampling total concentrations of individual protein species from a log-normal distribution with the mean as in the ODE model and $CV^2 = 0.5$ while keeping the remaining concentrations fixed. Interestingly, the variability of the response threshold in the HIF model is largely insensitive to variability of the majority of network components (Fig. 6B). The variability in only two protein concentrations, nuclear FIH and HIF-1β, translates to large CV^2 of response thresholds.

Discussion

Signalling networks can transform analog, continuous input signals into distinct low and high response states [47]. The sigmoidal shape of that response is typically a result of layers of phospho- and dephosphorylation cycles (e.g. MAPK cascade, [22]) or simply results from nonlinearity of enzymatic reactions as in case of the HIF network. The steep sigmoidal response minimises the region where stimuli could result in ambiguous outputs, making such a response characteristic a prevailing biological mechanism on

which cellular decision-making can rely. Because of the large number of molecules that eukaryotic signalling networks typically consist of, at the level of a single cell these systems seem to be protected from undesirable stochastic effects, which can occur at low molecule counts. Still, cells within a population differ in their molecular make-up because of the biochemical noise that affects total protein levels. This randomness affects the shape of the dose-response and causes a similarly random response of a cellular population.

Our theoretical results demonstrate that networks with sigmoidal response characteristics possess yet another fascinating feature, this time at the level of cellular ensemble. In the presence of variability in nonlinear dose-response across the population, two subpopulations can emerge with distinct response levels. The condition being, dose response needs to be of sufficient steepness. Our analysis provides intuitive mathematical insights into conditions under which such a response in form of a bimodal protein distribution may arise.

Cell-to-cell variability of the dose-response threshold, x_{50}, more commonly known as EC_{50}, is essential for generating wide or bimodal distributions in response to a common input signal. In the absence of such response variability, protein distribution would not widen but shift proportionally to the stimulus (Fig. 3A), which is not what we observed in our experiments. Flow-cytometric analysis of the HIF system demonstrated that the response, measured as ODD-GFP distribution, indeed widens for inputs (DMOG treatment) in the steepest region of the Hill-type dose-response. Our theoretical framework provides means of estimating EC_{50} variability from flow cytometry data and an explanation of protein distribution widening.

Without EC_{50} variability, the ODD-GFP distribution would not widen as is illustrated by the dotted line in figure 5D. Even though the squared coefficient of variation of the response threshold decreased 10 times between 4 and $16h$ after DMOG treatment, the steepness H of the response increased more than twice over the same period. Together these two parameters facilitate a necessary but not sufficient condition for bimodality expressed by equation (3). After substituting EC_{50} variability and H, we find that the system remains approximately in the same regime where only very mild bimodality may arise (Supplementary Table S6 and Supplementary Figure S6). Using our framework we hypothesise that the response steepness at $16h$ post-treatment is sufficient to bring about two distinct peaks in the response, provided that CV^2 of EC_{50} remained at the level of 2.72 (as estimated at $4h$) throughout the treatment (figure S6).

We have shown that due to certain features of the nonlinear input-output characteristics commonly observed in cellular signalling networks, random differences between individual cells enable the separation of these cells into subpopulations with distinct responses to the common signal. The significance of our results extends beyond cascaded signalling networks. Any network with nonlinear dose-response characteristics may exhibit bimodal behaviour as shown in our study. In particular, a simple enzymatic reaction or a gene expression network also belong to that class. For all of such nonlinear networks, variability of EC_{50} caused by cell-to-cell differences in protein concentrations is an important factor to consider when designing a perturbation, for example a drug treatment. According to our theory, one of the strategies to avoid the emergence of two subpopulations, low and high responders, is to smooth the dose response, i.e. decrease the coefficient H. This in turn can be achieved by establishing a negative feedback in the network [20]. Alternatively, the condition expressed by equation (3) demonstrates that the output protein distribution can be rid of bimodality by decreasing the variability of dose-response threshold resulting from cell-to-cell variability of network components. With current advancements in synthetic biology and ongoing progress in mathematical modelling of biochemical networks, such interventions in *in vivo* systems will likely become more routine. An intriguing open question is to what extent bimodal population-wide protein distributions brought about by the mechanism discussed here are employed to perform physiologically relevant decision-making.

Materials and Methods

Cell culture

Human Colon Carcinoma (HCT116) cells stably expressing GFP-ODD were a generous gift from Prof. Gottlieb and published [40]. The cells were subsequently sub-cloned as single-cell clones by growing cells in DMEM 10% FCS supplemented with $800\,\mu g/mL$ G418. The clones were treated with $2\,mM$ DMOG for 16 hours. Two clones where eGFP-ODD was induced were selected. Cells were then maintained in a humidified 5% CO_2 incubator at 37 °C and cultured in Dulbecco's modified Eagle's medium supplemented with 10% FCS, 1% L-glutamine, and $50\,\mu g/mL$ G418.

Flow cytometry

HCT116 cells were treated with cell permeable pan-hydroxylase inhibitor dimethyloxalylglycine (DMOG; Cayman Chemicals, Michigan, USA) dissolved in DMSO (Sigma, Wicklow, Ireland) and diluted with growth medium to appropriate concentration. The cells were then lifted by trypsinization (0.05% Trypsin-EDTA, Gibco) and resuspended in $0.5\,mL$ growth medium with DMOG concentration corresponding to initial stimulation. Experiments were replicated 4 times for each time point. The samples were analysed with Accuri C6. Post-gating by forward and side scatter was performed to remove events corresponding to dead cells, debris, and cell clusters (i.e. doublets). For each sample, 10000 events (cells) were collected in final gating.

Dose response from flow cytometry experiments (Fig. 5) was calculated using normalised median fluorescence intensity (nMFI),

$$\mathrm{nMFI}(\mathrm{stimulus}_i) = \frac{\text{median fluorescence}(\mathrm{stimulus}_i)}{\text{median fluorescence}(\mathrm{control})} \tag{5}$$

In order to quantify the width of protein distributions obtained from flow cytometry and calculated numerically, we use Robust CV (from FlowJo flow cytometry analysis software) defined as follows,

$$\mathrm{rCV} = \frac{100}{2} \cdot \frac{\mathrm{intensity}[84.13\ \%\mathrm{ile}] - \mathrm{intensity}[15.87\ \%\mathrm{ile}]}{\text{median intensity}} \tag{6}$$

The rCV is not as sensitive to outliers and gives a better than CV description of the distribution spread on logarithmic scales.

Acknowledgments

Supported by Science Foundation Ireland under Grant No. 06/CE/B1129 and European Union Grant PRIMES No. FP7-HEALTH-2011-278568. We thank Lisa Heiserich for kindly providing us with HCT116 cells and the anonymous reviewers for their insightful comments.

References

1. I. Golding and E. C. Cox, "RNA dynamics in live Escherichia coli cells.," *Proceedings of the National Academy of Sciences*, vol. 101, no. 31, pp. 11310–11315, 2004.

2. A. Raj, C. S. Peskin, D. Tranchina, D. Y. Vargas, and S. Tyagi, "Stochastic mRNA synthesis in mammalian cells," *PLoS Biol*, vol. 4, no. 10, p. e309, 2006.

3. J. R. S. Newman, S. Ghaemmaghami, J. Ihmels, D. K. Breslow, M. Noble, J. L. DeRisi, and J. S. Weissman, "Single-cell proteomic analysis of S. cerevisiae reveals the architecture of biological noise," *Nature*, vol. 441, no. 7095, pp. 840–846, 2006.

4. M. Bengtsson, M. Hemberg, P. Rorsman, and A. Ståhlberg, "Quantification of mRNA in single cells and modelling of RT-qPCR induced noise.," *BMC Mol. Biol.*, vol. 9, p. 63, 2008.

5. D. R. Tyson, S. P. Garbett, P. L. Frick, and V. Quaranta, "Fractional proliferation: a method to deconvolve cell population dynamics from single-cell data.," *Nature Methods*, vol. 9, no. 9, pp. 923–928, 2012.

6. W. J. Blake, G. Balázsi, M. A. Kohanski, F. J. Isaacs, K. F. Murphy, Y. Kuang, C. R. Cantor, D. R. Walt, and J. J. Collins, "Phenotypic consequences of promoter-mediated transcriptional noise.," *Molecular Cell*, vol. 24, no. 6, pp. 853–865, 2006.

7. A. A. Cohen, N. Geva-Zatorsky, E. Eden, M. Frenkel-Morgenstern, I. Issaeva, A. Sigal, R. Milo, C. Cohen-Saidon, Y. Liron, Z. Kam, L. Cohen, T. Danon, N. Perzov, and U. Alon, "Dynamic proteomics of individual cancer cells in response to a drug.," *Science*, vol. 322, no. 5907, pp. 1511–1516, 2008.

8. S. Gaudet, S. L. Spencer, W. W. Chen, and P. K. Sorger, "Exploring the contextual sensitivity of factors that determine cell-to-cell variability in receptor-mediated apoptosis.," *PLoS Comp. Biol.*, vol. 8, no. 4, p. e1002482, 2012.

9. V. Shahrezaei and P. S. Swain, "Analytical distributions for stochastic gene expression.," *PNAS*, vol. 105, no. 45, pp. 17256–17261, 2008.

10. A. Schwabe, M. Dobrzyński, K. Rybakova, P. Verschure, and F. J. Bruggeman, "Origins of stochastic intracellular processes and consequences for cell-to-cell variability and cellular survival strategies.," *Meth. Enzymol.*, vol. 500, pp. 597–625, 2011.

11. J. Yu, J. Xiao, X. Ren, K. Lao, and X. S. Xie, "Probing gene expression in live cells, one protein molecule at a time," *Science*, vol. 311, no. 5767, pp. 1600–1603, 2006.

12. W. J. Blake, M. Kærn, C. R. Cantor, and J. J. Collins, "Noise in eukaryotic gene expression," *Nature*, vol. 422, no. 6932, pp. 633–637, 2003.

13. A. Becskei, B. Séraphin, and L. Serrano, "Positive feedback in eukaryotic gene networks: cell differentiation by graded to binary response conversion," *The EMBO Journal*, vol. 20, no. 10, pp. 2528–2535, 2001.

14. B. N. Kholodenko, "Cell-signalling dynamics in time and space," *Nat Rev Mol Cell Biol*, vol. 7, no. 3, pp. 165–176, 2006.

15. J. J. Tyson, W. T. Baumann, C. Chen, A. Verdugo, I. Tavassoly, Y. Wang, L. M. Weiner, and R. Clarke, "Dynamic modelling of oestrogen signalling and cell fate in breast cancer cells," *Nat. Rev. Cancer*, vol. 11, no. 7, pp. 523–532, 2011.

16. D. Fey, D. R. Croucher, W. Kolch, and B. N. Kholodenko, "Crosstalk and signaling switches in mitogen-activated protein kinase cascades.," *Front Physiol*, vol. 3, p. 355, 2012.

17. J. J. Collins, T. S. Gardner, and C. R. Cantor, "Construction of a genetic toggle switch in Escherichia coli," *Nature*, vol. 403, no. 6767, pp. 339–342, 2000.

18. M. Samoilov, S. Plyasunov, and A. P. Arkin, "Stochastic amplification and signaling in enzymatic futile cycles through noise-induced bistability with oscillations.," *PNAS*, vol. 102, no. 7, pp. 2310–2315, 2005.

19. J. M. G. Vilar, "Noisy-threshold control of cell death," *BMC Syst Biol*, vol. 4, no. 1, p. 152, 2010.

20. M. R. Birtwistle, J. Rauch, A. Kiyatkin, E. Aksamitiene, M. Dobrzyński, J. B. Hoek, W. Kolch, B. A. Ogunnaike, and B. N. Kholodenko, "Emergence of bimodal cell population responses from the interplay between analog single-cell signaling and protein expression noise.," *BMC Syst Biol*, vol. 6, no. 1, p. 109, 2012.

21. M. Dobrzyński, D. Fey, L. K. Nguyen, and B. N. Kholodenko, "Bimodal protein distributions in heterogeneous oscillating systems," in *Computational Methods in Systems Biology* (D. Gilbert and M. Heiner, eds.), Lecture Notes in Computer Science, pp. 17–28, Springer Berlin Heidelberg, 2012.

22. C. Y. Huang and J. E. Ferrell, "Ultrasensitivity in the mitogen-activated protein kinase cascade," *Proceedings of the National Academy of Sciences of the United States of America*, vol. 93, no. 19, pp. 10078–10083, 1996.

23. J.-Y. Chen, J.-R. Lin, K. A. Cimprich, and T. Meyer, "A two-dimensional ERK-AKT signaling code for an NGF-triggered cell-fate decision.," *Molecular Cell*, vol. 45, no. 2, pp. 196–209, 2012.

24. S. Krishna, B. Banerjee, T. V. Ramakrishnan, and G. V. Shivashankar, "Stochastic simulations of the origins and implications of long-tailed distributions in gene expression," *PNAS*, vol. 102, no. 13, pp. 4771–4776, 2005.

25. C. Lu and R. D. King, "An investigation into the population abundance distribution of mRNAs, proteins, and metabolites in biological systems," *Bioinformatics*, vol. 25, no. 16, pp. 2020–2027, 2009.

26. M. R. Birtwistle, A. von Kriegsheim, M. Dobrzyński, B. N. Kholodenko, and W. Kolch, "Mammalian protein expression noise: scaling principles and the implications for knockdown experiments.," *Mol Biosyst*, vol. 8, no. 11, pp. 3068–3076, 2012.

27. M. Kærn, T. C. Elston, W. J. Blake, and J. J. Collins, "Stochasticity in gene expression: from theories to phenotypes," *Nat Rev Genet*, vol. 6, no. 6, pp. 451–64, 2005.

28. G. Tkacik, C. G. Callan, and W. Bialek, "Information flow and optimization in transcriptional regulation.," *PNAS*, vol. 105, no. 34, pp. 12265–12270, 2008.

29. A. M. Walczak, A. Mugler, and C. H. Wiggins, "A stochastic spectral analysis of transcriptional regulatory cascades.," *PNAS*, vol. 106, no. 16, pp. 6529–6534, 2009.

30. A. Ochab-Marcinek and M. Tabaka, "Bimodal gene expression in noncooperative regulatory systems.," *PNAS*, vol. 107, no. 51, pp. 22096–22101, 2010.

31. M. S. Bartlett, "Information maximization in face processing," *Neurocomputing*, vol. 70, no. 13, pp. 2204–2217, 2007.

32. S. Laughlin, "A simple coding procedure enhances a neuron's information capacity.," *Z. Naturforsch., C, Biosci.*, vol. 36, no. 9-10, pp. 910–912, 1981.

33. A. Lipshtat, G. Jayaraman, J. C. He, and R. Iyengar, "Design of versatile biochemical switches that respond to amplitude, duration, and spatial cues.," *PNAS*, vol. 107, no. 3, pp. 1247–1252, 2010.

34. J. E. Dueber, E. A. Mirsky, and W. A. Lim, "Engineering synthetic signaling proteins with ultrasensitive input/output control.," *Nat Biotechnol*, vol. 25, no. 6, pp. 660–662, 2007.

35. T. M. Cover and J. A. Thomas, "Entropy, Relative Entropy and Mutual Information," in *Elements of Information Theory*, pp. 12–49, New York: John Wiley & Sons, 1991.

36. G. L. Semenza, "Hypoxia-Inducible Factors in Physiology and Medicine," *Cell*, vol. 148, no. 3, pp. 399–408, 2012.

37. C. J. Schofield and P. J. Ratcliffe, "Oxygen sensing by HIF hydroxylases.," *Nat Rev Mol Cell Biol*, vol. 5, no. 5, pp. 343–354, 2004.

38. R. K. Bruick and S. L. McKnight, "A conserved family of prolyl-4-hydroxylases that modify HIF.," *Science*, vol. 294, no. 5545, pp. 1337–1340, 2001.

39. N. Masson, C. Willam, P. H. Maxwell, C. W. Pugh, and P. J. Ratcliffe, "Independent function of two destruction domains in hypoxia-inducible factor-alpha chains activated by prolyl hydroxylation.," *The EMBO Journal*, vol. 20, no. 18, pp. 5197–5206, 2001.

40. D. A. Tennant, C. Frezza, E. D. MacKenzie, Q. D. Nguyen, L. Zheng, M. A. Selak, D. L. Roberts, C. Dive, D. G. Watson, E. O. Aboagye, and E. Gottlieb, "Reactivating HIF prolyl hydroxylases under hypoxia results in metabolic catastrophe and cell death.," *Oncogene*, vol. 28, no. 45, pp. 4009–4021, 2009.

41. A. C. Epstein, J. M. Gleadle, L. A. McNeill, K. S. Hewitson, J. O'Rourke, D. R. Mole, M. Mukherji, E. Metzen, M. I. Wilson, A. Dhanda, Y. M. Tian, N. Masson, D. L. Hamilton, P. Jaakkola, R. Barstead, J. Hodgkin, P. H. Maxwell, C. W. Pugh, C. J. Schofield, and P. J. Ratcliffe, "C. elegans EGL-9 and mammalian homologs define a family of dioxygenases that regulate HIF by prolyl hydroxylation.," *Cell*, vol. 107, no. 1, pp. 43–54, 2001.

42. L. K. Nguyen, M. A. S. Cavadas, C. C. Scholz, S. F. Fitzpatrick, U. Bruning, E. P. Cummins, M. M. Tambuwala, M. C. Manresa, B. N. Kholodenko, C. T. Taylor, and A. Cheong, "A dynamic model of the hypoxia-inducible factor 1α (HIF-1α) network.," *J Cell Sci*, vol. 126, no. Pt 6, pp. 1454–1463, 2013.

43. H. Akaike, "A new look at the statistical model identification," *Automatic Control, IEEE Transactions on*, vol. 19, no. 6, pp. 716–723, 1974.

44. O. Feinerman, J. Veiga, J. R. Dorfman, R. N. Germain, and G. Altan-Bonnet, "Variability and robustness in T cell activation from regulated heterogeneity in protein levels.," *Science*, vol. 321, no. 5892, pp. 1081–1084, 2008.

45. M. Niepel, S. L. Spencer, and P. K. Sorger, "Non-genetic cell-to-cell variability and the consequences for pharmacology.," *Curr Opin Chem Biol*, vol. 13, no. 5-6, pp. 556–561, 2009.

46. S. L. Spencer, S. Gaudet, J. G. Albeck, J. M. Burke, and P. K. Sorger, "Non-genetic origins of cell-to-cell variability in TRAIL-induced apoptosis.," *Nature*, vol. 459, no. 7245, pp. 428–432, 2009.

47. B. N. Kholodenko, J. F. Hancock, and W. Kolch, "Signalling ballet in space and time.," *Nat Rev Mol Cell Biol*, vol. 11, no. 6, pp. 414–426, 2010.

48. T. M. Cover and J. A. Thomas, "Differential Entropy," in *Elements of Information Theory*, pp. 224–238, New York: John Wiley & Sons, 1991.

Figure captions

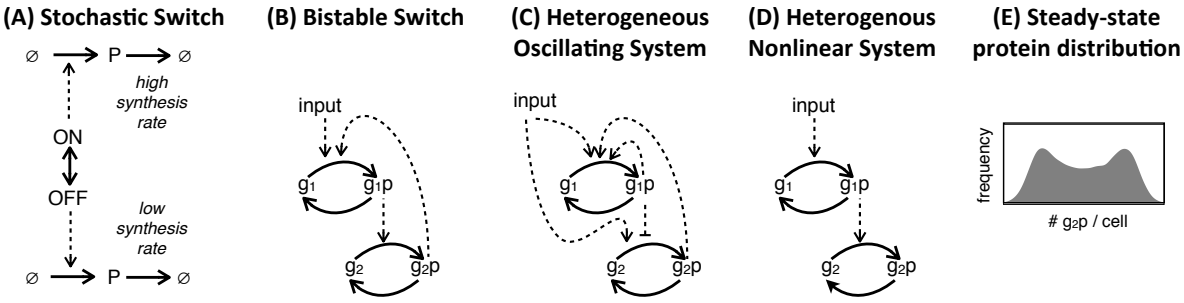

Figure 1. Generic mechanisms that can give rise to bimodal steady-state protein distributions on the cell population level. (A) Spontaneous switching between active and inactive state of the promotor [10]. (B) Network bistability is brought about by positive feedback [13, 15, 16]. (C) Oscillating protein abundances in the presence of cell-to-cell variability in oscillations period and (or) phase [21]. (D) A network with nonlinear input-output characteristic subject to intrinsic and (or) extrinsic noise [20, 30, 45]. (E) An example of a histogram of steady-state protein concentrations from individual cells as obtained with flow cytometry. Bimodality can arise in the population of cells driven by any of the mechanisms shown in panels A-D.

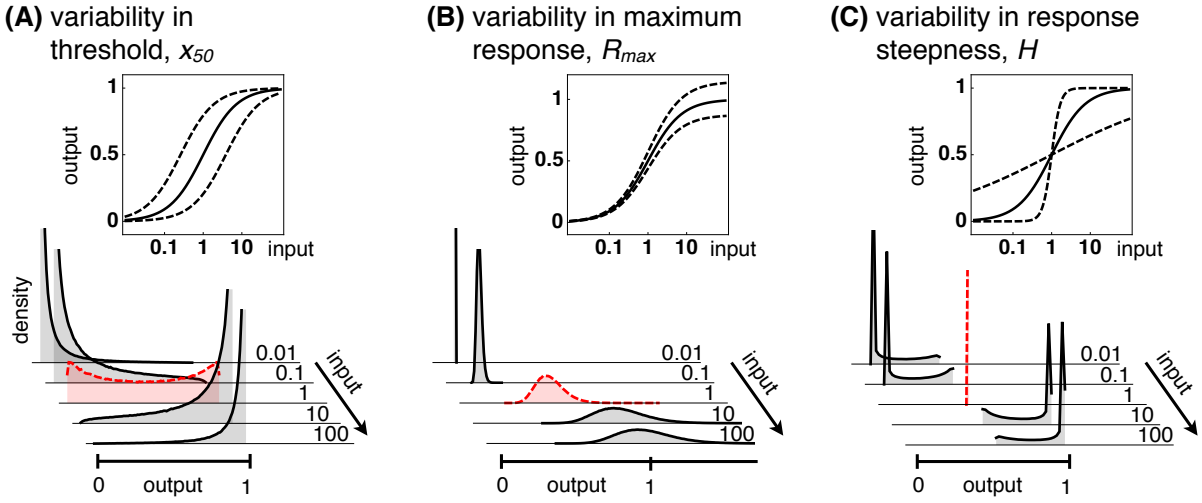

Figure 2. Protein distributions arising from variability of different parameters in the Hill-type response of a nonlinear network. Solid lines in upper panels – response function from equation (1) with $\beta = 0$, $x_{50} = 1$, $R_{max} = 1$, $H = 1$. Dashed lines indicate the middle 50% of dose-responses when the indicated parameter is randomly sampled from a log-normal distribution with (A) median, $m_{x50} = 1$ and shape parameter $\sigma_{x50} = 2$, (B) $m_{Rmax} = 1$, $\sigma_{Rmax} = 0.2$ (C) $m_H = 1$, $\sigma_H = 2$. Shown in bottom panels are output distributions for a range of inputs. Red dashed – distribution for the input stimulus $x = 1$, which is the midpoint of the averaged dose-response.

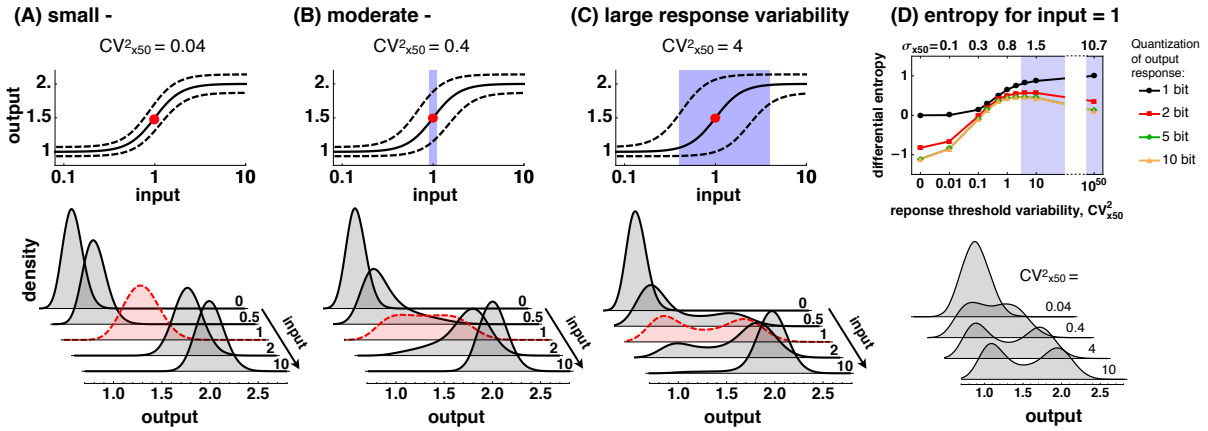

Figure 3. The effect of variability in the response threshold on protein activity distributions. The response steepness $H = 3$. The response threshold is drawn from a log-normal distribution with median $m_{x50} = 1$ and shape parameter $\sigma_{x50} = 0.20$, 0.58 and 1.27 for panels A-C, respectively. Also log-normally distributed is the baseline, ($m_\beta = 1$, $\sigma_\beta = 0.1$), and maximum response, ($m_{Rmax} = 1$, $\sigma_{Rmax} = 0.1$). Dashed lines on both sides of the dose-response (solid line) indicate the middle 50% of responses resulting from variability in β, R_{max}, and x_{50}. Red dot is the midpoint (half-maximum) of the dose-response. (D) Differential entropy of output distributions for input level 1 (red dot in panels A-C) as function of threshold variability. Since distributions in A-C are sampled numerically, Shannon entropy is calculated for decreasing histogram bin sizes dy (or increasing quantisations n such that $dy = 1/2^n$) to give the best approximation of the entropy of the continuous density, i.e. the differential entropy [48]. The differential entropy is approximately Shannon entropy of an n-bit quantisation of the varying response level, minus n. (A-D) Shaded regions indicate the range of inputs for which the distributions become bimodal and the value of *pdf* at the antimode is lower than 97% of the *pdf*'s value at the minor mode.

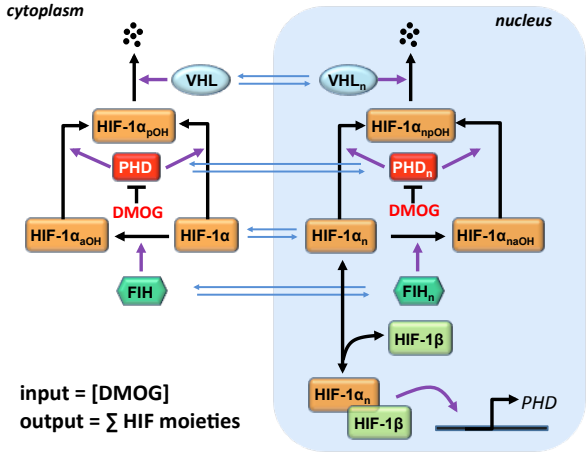

Figure 4. Simplified scheme of the HIF signalling pathway. In both cytoplasm and nucleus (subscript n), HIF-1α can be asparaginyl-hydroxylated (aOH) by Factor Inhibiting HIF (FIH) and/or prolyl-hydroxylated (pOH) by prolyl-hydroxylases (PHD). Prolyl-hydroxylated HIF-1α is targeted for Von Hippel-Lindau (VHL) mediated degradation while asparaginyl-hydroxylated HIF-1α prevents its transcriptional activity. Under DMOG (or hypoxia), PHD is inactivated, leading to HIF-1α protein stabilisation and translocation to the nucleus. HIF-1α, PHD, FIH and VHL can shuttle between the nucleus and cytoplasm. Nuclear HIF-1α dimerises with HIF-1β, creating a transcriptional complex which can bind to the HIF-response elements (HRE) of the target genes, including that of PHD, leading to upregulation of PHD protein and generating a negative feedback loop.

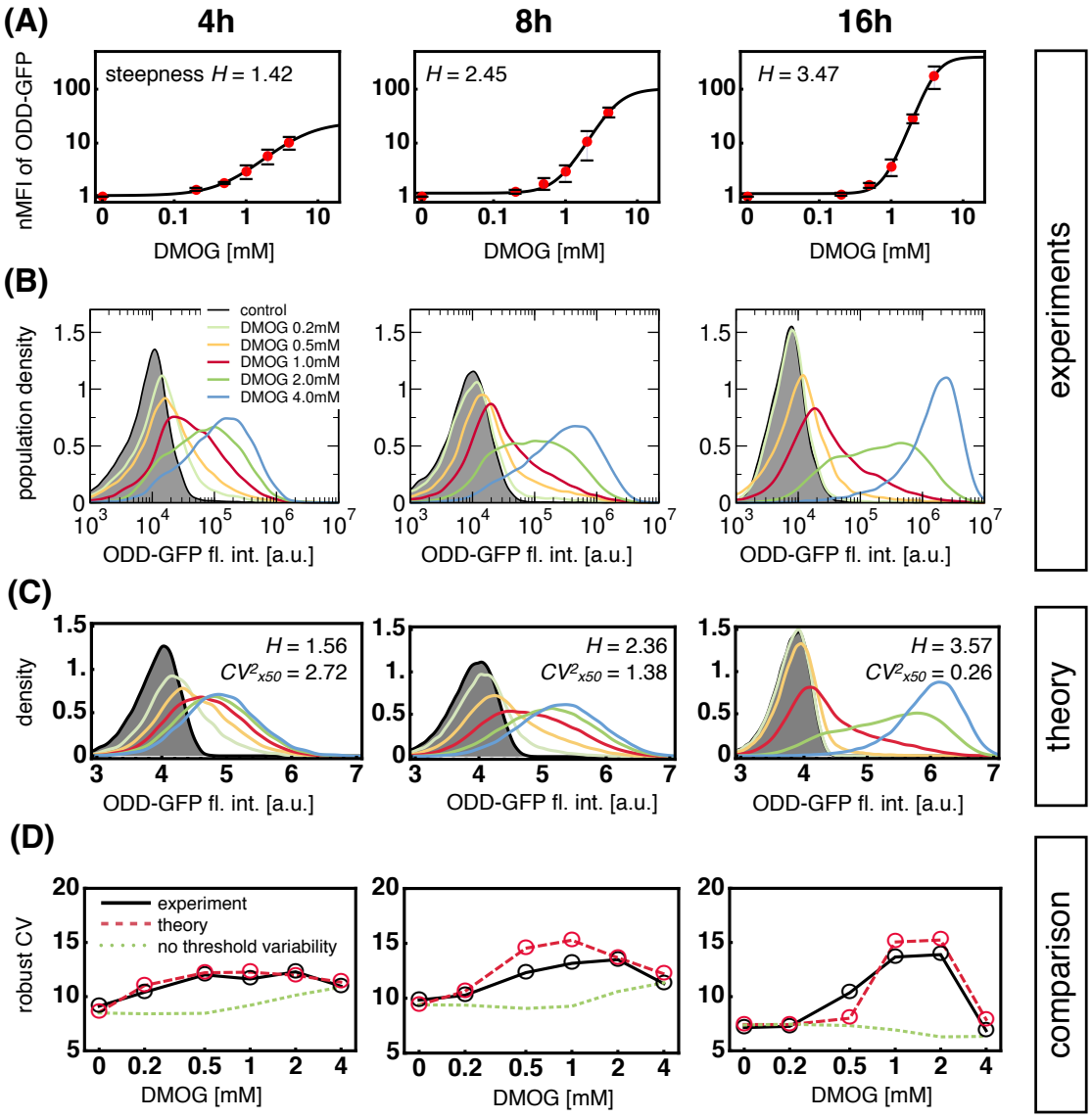

Figure 5. Experimental and theoretical ODD-GFP concentration distributions due to DMOG treatment in the HIF response system. (A) Dose response of ODD-GFP to DMOG. Points – flow-cytometric measurement of normalised median fluorescence intensity (nMFI), equation (5) in Materials and Methods, averaged over 3 or 4 biological replicates. Error bars indicate 1 SD. Solid lines – best fits of the Hill equation (1). Fitting parameters listed in Table S1. (B) Flow-cytometric measurement of ODD-GFP fluorescence intensity (FL1-A) obtained from a single biological repeat at 4, 8 and 16h post-DMOG. Calculated from 10000 cells in final gating. (C) ODD-GFP distributions computed by Monte Carlo sampling of equation (1). Distributions of Hill parameters are fitted to experimental data from row B. Shown are fitted values of H and CV^2 = variance/mean^2 of the threshold distribution. See Supplementary Figure S5 and Tables S2-S5. (D) Solid line – robust CV (rCV), equation (6) in Materials and Methods, for experimental data from row B. Dashed line – rCV for theoretical ODD-GFP concentration distributions from row C. Dotted line – rCV with variability in response thresholds, σ_{x50}, set to zero and the mean set to the mean of the fitted threshold distribution.

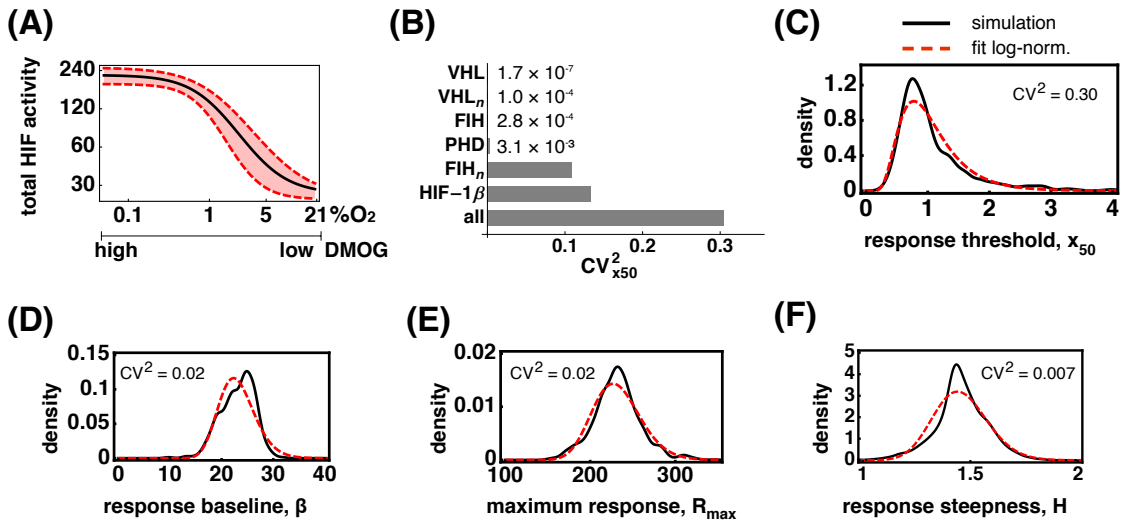

Figure 6. Mathematical model of HIF system demonstrates the effect of variability in protein concentrations on the dose-response. Using a published ODE model [42] we calculate the dose-response at $16h$ post-DMOG for an ensemble of systems where the total protein levels are drawn from a log-normal distribution with $CV^2 = 0.5$ and mean: $[\text{VHL}] = 50\,nM$, $[\text{VHL}_n] = 50\,nM$, $[\text{FIH}] = 110\,nM$, $[\text{PHD}] = 100\,nM$, $[\text{FIH}_n] = 40\,nM$, $[\text{HIF-1}\beta] = 170\,nM$. For each of the simulated dose responses we fit a Hill function: $\beta + R_{max}\, x_{50}^H/(x_{50}^H + x^H)$ and obtain the corresponding parameters. (A) Black solid line – the mean response to oxygen level: 21% – normoxia, below 1% – hypoxia (note log scale of x-axis). All protein levels are varied. Red dashed line – 1 SD. (B) CV^2 of the response threshold resulting from variability in individual and all protein levels. (C-F) Black solid line – simulated probability densities of Hill parameters obtained from an ensemble of fitted Hill functions when all total protein levels are drawn from a log-normal distribution with $CV^2 = 0.5$ (lowest bar in panel B). Red dashed line – best fit of the log-normal distribution.

Supplementary Information for: Nonlinear signalling networks and cell-to-cell variability transform external signals into broadly distributed or bimodal responses

Maciej Dobrzyński, Lan K. Nguyen, Marc R. Birtwistle,
Alexander von Kriegsheim, Alfonso Blanco-Fernández,
Alex Cheong, Walter Kolch, Boris N. Kholodenko

June 5, 2014

1 Derivation of Equation 2 in the main text

A new random variable Y results from transformation of the existing random variable Z using a function $R(Z)$. The probability density function, *pdf*, of random variable Z is known and expressed as $f_Z(z)$. The goal is to obtain the *pdf* of Y, $f_Y(y)$ [1]. In our case, random variable Z represents cell-to-cell variability of the parameters that describe the response function $R(X)$, i.e. the input stimulus x, response threshold x_{50}, maximum response R_{max}, basal response β or response steepness H. For our purposes, the *pdf* $f_X(x)$ is a log-normal distribution.

The cumulative distribution function, CDF, of Y, can be expressed as:

$$F_Y(y) = P[Y \leq y] = P[R(Z) \leq y] = P[Z \in D_Y], \tag{1}$$

where the set $D_Y = z : R(Z) \leq y = z : z \leq r(y)$, where $r(y)$ is the inverse function of R. Equipped with these definitions we can express the CDF of Y in terms of the CDF of Z:

$$F_Y(y) = P[Z \leq r(y)] = F_Z(r(y)). \tag{2}$$

In order to obtain the *pdf* we simply differentiate the above expression to obtain:

$$f_Y(y) = \frac{d}{dy} F_Y(y) = f_Z(r(y)) \frac{d}{dy} r(y). \tag{3}$$

Assumptions behind the above equation, monotonicity of $R(z)$ and finite integral of f_z, are easily satisfied in a biological system such as a signalling network. The response function $R(z)$ is typically approximated by a sigmoidal Hill function:

$$y = R(x, \beta, \theta, R_{max}, H) = \beta + R_{max} \frac{x^H}{x_{50}^H + x^H}\,. \tag{4}$$

Parameter variability described by the function f_z is a probability density function which by definition sums up (integrates) to 1.

2 Conditions for the existence of bimodality in the presence of response threshold variability

In this section we derive conditions for existence of bimodal output distribution given log-normal distribution of the response threshold x_{50} with scale parameter μ_{x50} and shape parameter σ_{x50},

$$f_{X_{50}}(x_{50}) = \frac{1}{x_{50}\,\sigma_{x50}\,\sqrt{2\pi}} \exp\left[-\left(\log x_{50} - \mu_{x50}\right)^2 / 2\sigma_{x50}^2\right], \quad x_{50} > 0, \tag{5}$$

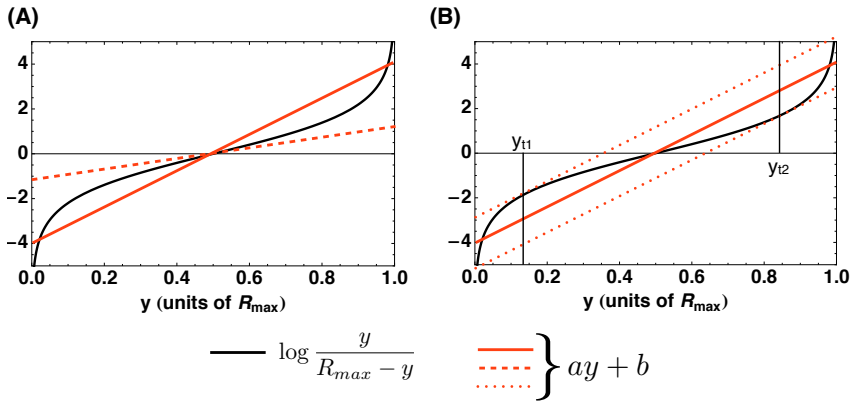

Figure S1: Graphical interpretation of conditions for the existence of bimodality. Equation 8 has solutions in terms of variable y when expressions on the left and the right hand side intersect. (A) First condition assures the slope of the linear function $ay+b$ on the left hand side of Eq. 8. Only lines with slopes larger than $4/R_{max}$ (solid red) are able to intersect the log function (solid black) three times. (B) Appropriate slope is yet not sufficient; y-intercept of the linear function, as quantified by b, has to be within certain bounds (Eq. 12).

and sigmoidal response modelled by Hill function (Eq. 4). Substituting the above into Eq. 3, we obtain:

$$f_{out}(\mathbf{y}) = \frac{1}{H\sigma_{x50}\sqrt{2\pi}} \frac{R_{max}}{(R_{max}-\mathbf{y})\mathbf{y}} \exp\left[-\frac{1}{2\sigma_{x50}^2}\left(\mu_{x50} - \log\left[x\left(\frac{R_{max}-\mathbf{y}}{\mathbf{y}}\right)^{\frac{1}{H}}\right]\right)^2\right] . \tag{6}$$

For ease of read, we set the type of the output y in bold.

A bimodal distribution exists only if the above function assumes two maxima and a minimum between them. In order to find these three extrema we analyse first derivative of Eq. 6:

$$\begin{aligned}\frac{d}{dy} f_{out}(\mathbf{y}) &= \frac{1}{H^2\sigma_{x50}^3\sqrt{2\pi}} \frac{R_{max}^2}{(R_{max}-\mathbf{y})^2\,\mathbf{y}^2} \exp\left[-(\dots)^2\right] \\ &\times \left(\frac{2H\sigma_{x50}^2}{R_{max}}\mathbf{y} - \mu_{x50} - H\sigma_{x50}^2 + \log\left[x\left(\frac{R_{max}-\mathbf{y}}{\mathbf{y}}\right)^{\frac{1}{H}}\right]\right) .\end{aligned} \tag{7}$$

The term with the exponent is always positive, therefore we only analyse the expression in brackets and search for its zeros. After expanding logarithm on the right hand side, we obtain:

$$\frac{2H^2\sigma_{x50}^2}{R_{max}}\mathbf{y} - H^2\sigma_{x50}^2 + H\left(\log x - \mu_{x50}\right) = \log\left[\frac{\mathbf{y}}{R_{max}-\mathbf{y}}\right] , \tag{8}$$

which is a transcendental equation with a linear function of the form $ay+b$ on the left hand side. We solve this equation graphically as shown in Fig. S1, which results in two conditions, for the slope a (panel A) and for y-intercept b (panel B).

The slope $a = 2H^2\sigma_{x50}^2/R_{max}$ has to be larger than the smallest slope of the r.h.s. of Eq. 8, which is achieved at the inflection point at $y = R_{max}/2$:

$$\frac{d}{dy}\log\left[\frac{\mathbf{y}}{R_{max}-\mathbf{y}}\right]\Bigg|_{y=R_{max}/2} = \frac{4}{R_{max}} . \tag{9}$$

This way we obtain the first condition, necessary but not sufficient, for the existence of bimodal output distribution,

$$H^2\sigma_{x50}^2 > 2 . \tag{10}$$

Note that the condition is independent of R_{max}.

Once we know the slope, we can search for the range of admissible y-intercepts that result in three intersections (Fig. S1). To achieve that, we first calculate argument y for which the slopes (first derivatives)

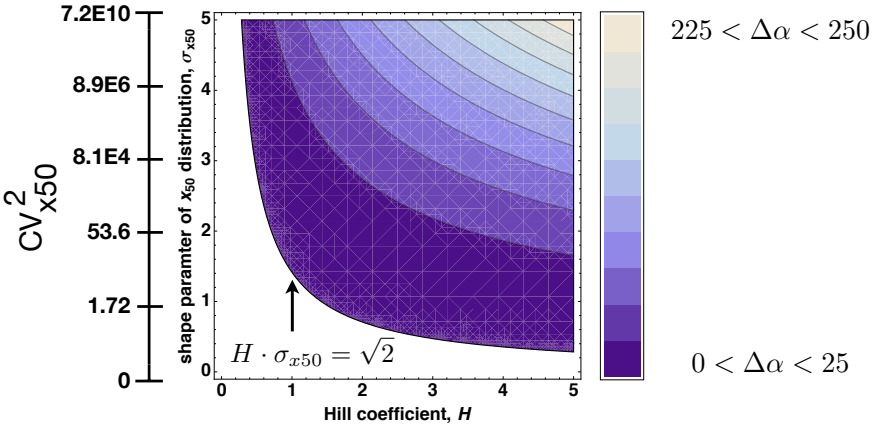

Figure S2: Bimodality region as function of Hill coefficient, H, and shape parameter of the x_{50} distribution, σ_{x50}. Colour coding indicates the width, $\Delta\alpha \equiv \alpha^+ - \alpha^-$, of admissible $\log(x/m_{x50})$ ratios that yield a bimodal distribution. The entire coloured region corresponds to the first condition, $H \cdot \sigma_{x50} > \sqrt{2}$.

of the left and the right hand side of Eq. 8 are equal; since the r.h.s. of Eq. 8 is symmetric around $R_{max}/2$, we obtain abscissae $y_{t1,t2}$ of two tangent points (cf. Fig. S1B),

$$\frac{2H^2\sigma_{x50}^2}{R_{max}} = \frac{R_{max}}{\mathbf{y}(R_{max}-\mathbf{y})} \quad \Longrightarrow \quad \mathbf{y_{t1,t2}} = \frac{R_{max}}{2}\left(1 \mp \sqrt{1 - \frac{2}{H^2\sigma_{x50}^2}}\right) . \tag{11}$$

By evaluating r.h.s. of Eq. 8 at y_{t1} and y_{t2} we obtain the lower and upper bound for parameter $b = H(\log x - \mu_{x50}) - H^2\sigma_{x50}^2$,

$$\begin{aligned} a\mathbf{y} + b\Big|_{y=y_{t1}} &< \log\left[\frac{\mathbf{y}}{R_{max}-\mathbf{y}}\right]\Big|_{y=y_{t1}} \\ a\mathbf{y} + b\Big|_{y=y_{t2}} &> \log\left[\frac{\mathbf{y}}{R_{max}-\mathbf{y}}\right]\Big|_{y=y_{t2}} . \end{aligned} \tag{12}$$

Before spelling out the result we rewrite parameter b by noting that $\mu_{x50} = \log m_{x50}$, where m_{x50} is the median of the log-normal distribution of the response parameter x_{50}. Therefore b becomes:

$$b = H \log\frac{x}{m_{x50}} - H^2\sigma_X^2 . \tag{13}$$

The median of a probability distribution is a half-maximum point of the related cumulative distribution. In other words, the median is the "middle point" of the distribution. Therefore, the fraction x/m_{x50} is the ratio of the input signal x and the middle point of the x_{50} distribution.

From Eq. 12 we derive symmetric bounds for logarithm of this ratio:

$$\alpha^-(H, \sigma_{x50}) < \log\frac{x}{m_{x50}} < \alpha^+(H, \sigma_{x50}) , \tag{14}$$

where:

$$\alpha^\pm(H, \sigma_{x50}) \equiv \pm\sigma_{x50}\sqrt{H^2\sigma_{x50}^2 - 2} + \frac{1}{H}\log\left[H^2\sigma_{x50}^2 - 1 \mp H\sigma_{x50}\sqrt{H^2\sigma_{x50}^2 - 2}\right] . \tag{15}$$

Figure S2 illustrates graphically the range of H and σ_{x50} parameters (Eq. 10) and the range of $\log(x/m_{x50})$ ratios (Eq. 14) that need to be satisfied in order to obtain a bimodal output distribution.

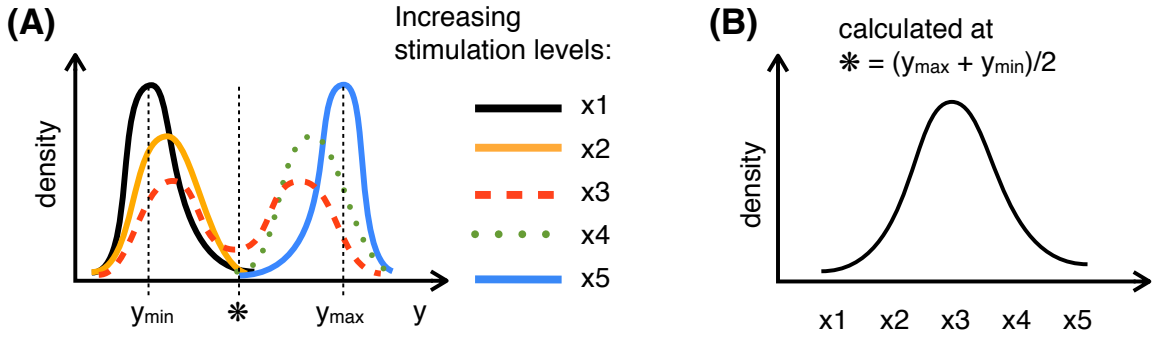

Figure S3: Schematic illustration of how to calculate x_{50} distribution from output distributions obtained for the range of inputs x. (A) First, create a function g_{cut} of input x, which assumes values of density (or frequency) for a particular output y. (B) We choose y at a half-distance between the peaks (the modes) of output distributions obtained for the saturating and basal levels of x. At $y = (R_{max} + \beta)/2$, the function g_{cut} depends only on parameters of x_{50} distribution (Eq. 17) which is assumed to be log-normal.

3 Inferring x_{50} distribution from output distributions

Consider Eq. 6 as a function of the input level x instead of the output y (Fig. S3). After normalisation to 1, such a function becomes a *pdf*:

$$\begin{aligned} g_{cut}(\mathbf{x};\, y,\, m_{x50},\, \sigma_{x50}) \quad &= \quad \frac{1}{m_{x50}\sigma_{x50}\sqrt{2\pi}} \left(\frac{R_{max}-y}{y}\right)^{1/H} \\ &\times \quad \exp\left[-\frac{\sigma_{x50}^2}{2} - \frac{1}{2\sigma_{x50}^2}\left(\mu_{x50} - \log\left[\mathbf{x}\left(\frac{R_{max}-y}{y}\right)^{1/H}\right]\right)^2\right]. \end{aligned} \tag{16}$$

This equation has the output value y as a parameter and the remaining problem is the choice of y such that the *pdf* depends only on parameters determining the underlying log-normal distribution of x_{50}, thus $m_{x50} = \exp(\mu_{x50})$ and σ_{x50}. The dependency on H and R_{max} can be alleviated by setting $y = R_{max}/2$. Therefore, the expression in parentheses, $(R_{max} - y)/y$, becomes 1 which yields:

$$g_{cut}\left(\mathbf{x};\, m_{x50},\, \sigma_{x50}\right)\Big|_{y=R_{max}/2} = \frac{1}{m_{x_{50}}\sigma_{x_{50}}\sqrt{2\pi}} \exp\left[-\frac{\sigma_{x_{50}}^2}{2} - \frac{1}{2\sigma_{x_{50}}^2}\log^2\left[\frac{m_{x50}}{\mathbf{x}}\right]\right]. \tag{17}$$

The above result demonstrates how to obtain parameters of the underlying log-normal distribution of threshold parameter x_{50} in the Hill response model. First, values of experimental output distributions obtained for a range of input levels x need to be taken at y equal to half of the maximum response R_{max}. Such a set can be fitted to equation 17 to obtain m_{x50} and σ_{x50}. The function 17 is not the distribution of x_{50}, but describes how the midpoint of the output distribution depends on input x. From this dependency parameter values of the underlying x_{50} distribution can be inferred from experimental results. By taking values of distributions obtained from flow cytometry at half-maximal response, the threshold variability with least dependence on other parameters of the dose-response can be estimated.

4 Distribution of Hill parameters

We take a generic model of a two-level cascade (Fig. S4A) with the following Michaelis-Menten kinetics to demonstrate the log-normal character of parameter distributions in the Hill approximation of the dose response:

$$g_1 \rightarrow g_1p: \ [g_{IN}]\ v_1 \frac{[g_1]}{k_1 + [g_1]} \tag{18a}$$

$$g_1p \rightarrow g_1: \ v_2 \frac{[g_1p]}{k_2 + [g_1p]} \tag{18b}$$

$$g_2 \rightarrow g_2p: \ [g_1p]\ v_3 \frac{[g_2]}{k_3 + [g_2]} \tag{18c}$$

$$g_2p \rightarrow g_2: \ v_4 \frac{[g_2p]}{k_4 + [g_2p]} \tag{18d}$$

The distribution of Hill parameters results from a distribution of total protein levels: $[g_1]_{tot} = [g_1] + [g_1p]$ and $[g_2]_{tot} = [g_2] + [g_2p]$. We take the following parameters: $v_1 = 1.8$, $v_2 = 9.5$, $v_3 = 0.8$, $v_4 = 2.6$, $k_1 = 9$, $k_2 = 3.7$, $k_3 = 5.4$, $k_4 = 7.2$.

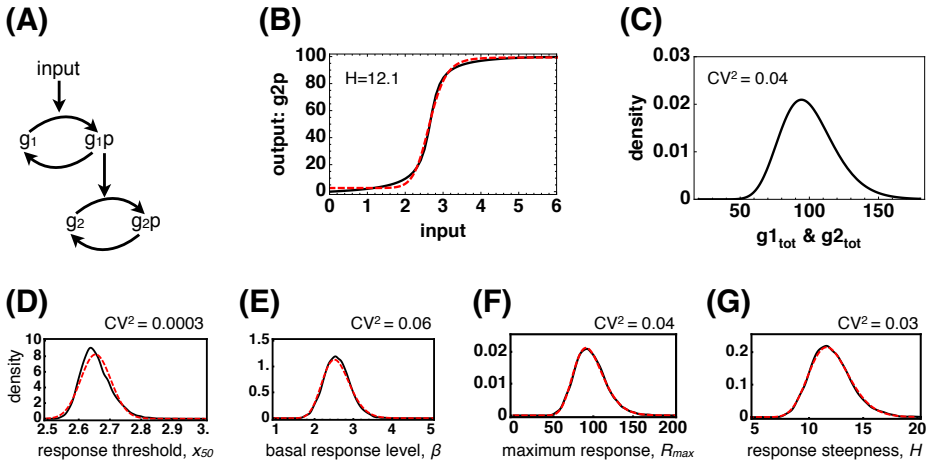

Figure S4: Distribution of parameters in Hill response model. (A) A generic two-level cascade. (B) Solid black line – steady-state dose-response of g_2p to input stimulation from analytical solution for $[g_1]_{tot} = [g_2]_{tot} = 100$; dashed red – fit of the Hill response function (Eq. 4), $\beta = 2.7$, $R_{max} = 96.6$, $x_{50} = 2.6$, $H = 12.1$. (C) Assumed log-normal distribution of g_1 and g_2 total levels with the mean 100 and the standard deviation 20. (D-G) Solid black line – distributions of response threshold x_{50}, basal response β, maximum response R_{max}, and response steepness H, respectively. Steady-state dose-responses were calculated for a range of inputs from the analytical solution with total $g_{1,2}$ levels sampled from the log-normal distribution shown in panel C. Then, in order to obtain parameter distributions, Hill functions were fitted to every dose-response. Dashed red line – fit of a log-normal distribution.

5 Fitting parameters of the Hill response model to experiments

The theoretical prediction of distributions shown in Figure 5C (main text) is based on fitting Hill response parameters to flow cytometry results shown in panel B of that figure. Steepness coefficient H is obtained by fitting Hill curve to normalised mean fluorescence intensity (nMFI) of ODD-GFP (Fig. S5A and Table S2). Other parameters are assumed to vary according to distributions fitted to flow cytometry data.

The variability in basal level β is assumed to follow a distribution of fluorescence intensity for unstimulated case, i.e. DMOG = $0mM$ (Fig. S5B and Table S3). The maximum response R_{max} varies as the distribution for the maximum stimulation in our experiments, i.e. DMOG = $4mM$ (Fig. S5C). We correct this distribution for the variability in basal level by subtracting the mean and variance of the latter (Table S4).

The threshold x_{50}, the only parameter that we assume to give rise to widening of the output distribution at intermediate stimuli level, is obtained according to procedure described in Section 3: values of ODD-GFP distributions for all DMOG stimuli are taken at approximately half maximum fluorescence intensity (Fig. S5D and Table S5).

We used the following probability density functions for the fitting procedure:

Log-normal distribution with shape parameter σ and scale parameter μ:

$$f_{LN}(x;\mu,\sigma) = \frac{1}{x\sqrt{2\pi}\sigma} e^{-\frac{(\ln x-\mu)^2}{2\sigma^2}} \tag{19}$$

Gamma distribution with shape parameter k and scale parameter θ:

$$f_G(x;k,\theta) = \frac{1}{\Gamma(k)\theta^k} x^{k-1} e^{-x/\theta} \tag{20}$$

Weibull distribution with shape parameter k and scale parameter λ:

$$f_W(x;k,\lambda) = \frac{k}{\lambda}\left(\frac{x}{\lambda}\right)^{k-1} e^{-(x/\lambda)^k} \tag{21}$$

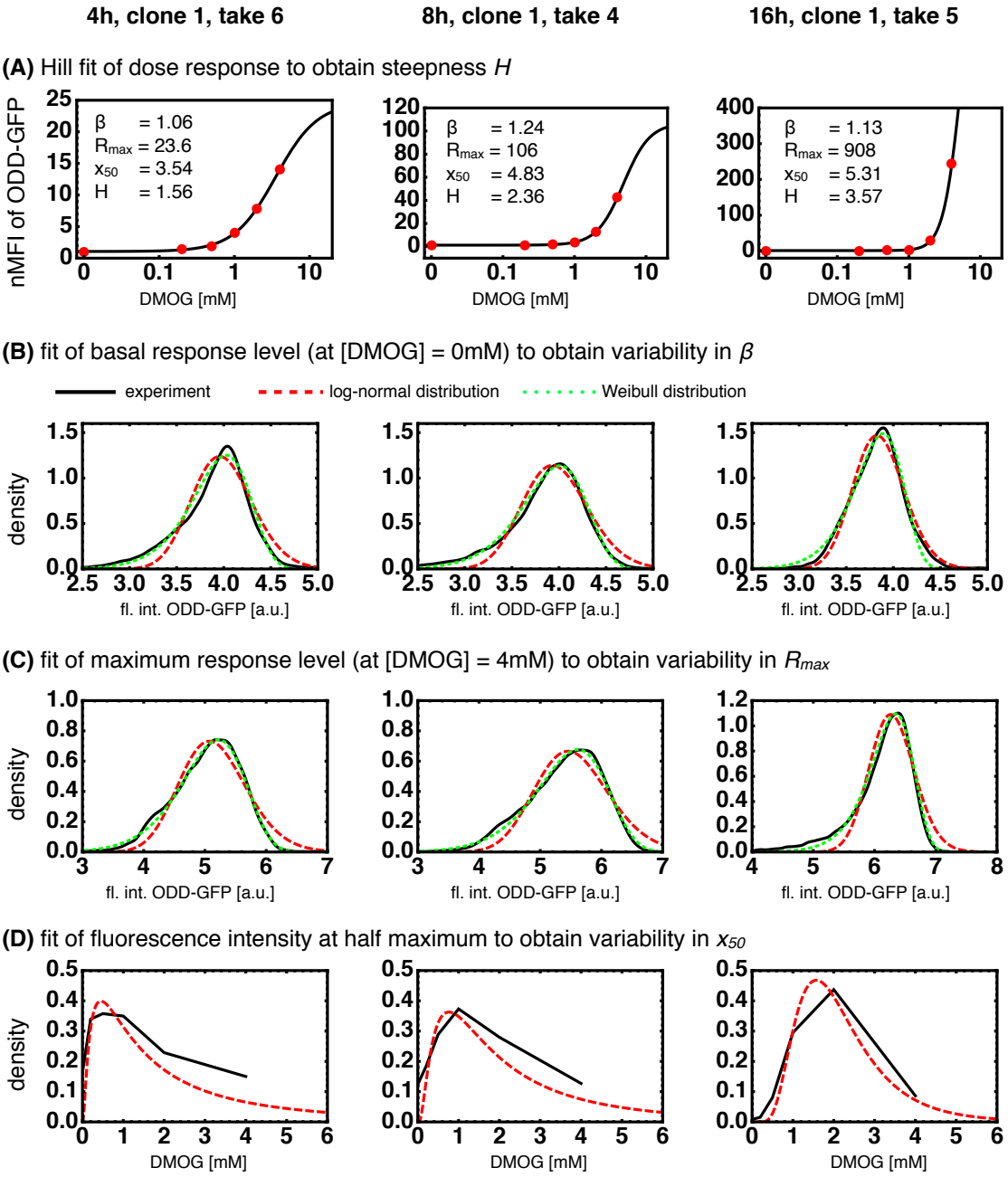

Figure S5: Fitting parameters of Hill response model to single flow cytometry measurements shown in Figure 5B (main text). (A) Red points – normalised median fluorescence intensity (nMFI, Eq. 5, main text) of ODD-GFP; solid line – fitted Hill response function (Eq. 4). Fitting parameters are β, R_{max}, x_{50} and H that correspond to basal level, maximum response, response threshold and response steepness, respectively. Fitting parameters are listed in Table S2. (B) Fits to ODD-GFP fluorescence intensity distributions for unstimulated case, which is a proxy of variability in β. (C) Fits to ODD-GFP fluorescence intensity distributions for maximum stimulation case, which is a proxy of variability in R_{max}. (B-D) Solid black line – experimental data. (B & C) Dashed red – log-normal distribution, dotted green – Weibull distribution. Weibull distribution was a better fit based on a smaller value of Akaike information criterion (AIC) as listed in Tables S3 & S4. (D) Fits to values of ODD-GFP fluorescence intensity distributions at approximately half maximum of the distance between medians of distributions recorded for DMOG $= 0mM$ and DMOG $= 4mM$, i.e. at $10^{4.4}$, $10^{4.5}$, 10^{5} for 4, 8 and 16h, respectively. Dashed red – $g_{cut}(x)$ distribution from Eq. 17 from which we obtain μ_{x50} and σ_{x50} of the underlying log-normal threshold distribution as listed in Table S5.

Table S1: Parameters of the response function, Eq. 4, fitted to averages over 3-4 biological repeats and shown in Fig. 5A, main text.

Time	Parameter	Estimate	Std.Err.	95% CI
4h	β	1.06	0.0785	(0.724, 1.40)
	R_{max}	23.5	5.69	(-0.958, 48.0)
	x_{50}	5.43	1.63	(-0.157, 12.4)
	H	1.42	0.124	(0.881, 1.95)
8h	β	1.18	0.153	(0.524, 1.84)
	R_{max}	101	40.5	(-73.7, 275)
	x_{50}	5.07	1.42	(-1.03, 11.2)
	H	2.45	0.263	(1.32, 3.58)
16h	β	1.16	0.131	(0.592, 1.72)
	R_{max}	394	56.1	(152, 635)
	x_{50}	4.24	0.326	(2.83, 5.64)
	H	3.47	0.154	(2.81, 4.14)

Table S2: Parameters of the response function, Eq. 4, fitted to a single experiment (Fig.S5A). We use fitted values of the steepness parameter H to predict ODD-GFP distributions in Fig. 5C, main text.

Time	Parameter	Estimate	Std.Err.	95% CI
4h	β	1.06	0.168	(0.339, 1.79)
	R_{max}	23.6	4.74	(3.21, 44.0)
	x_{50}	3.54	0.899	(-0.329, 7.41)
	H	1.56	0.192	(0.737, 2.39)
8h	β	1.24	0.245	(0.181, 2.29)
	R_{max}	106	44.5	(-85.4, 297)
	x_{50}	4.83	1.52	(-1.70, 11.4)
	H	2.36	0.308	(1.03, 3.68)
16h	β	1.13	0.125	(0.595, 1.67)
	R_{max}	908	304	(-399, 2214)
	x_{50}	5.31	0.746	(2.10, 8.51)
	H	3.57	0.163	(2.87, 4.27)

Table S3: Fitting parameters of the basal response level, [DMOG] = 0 mM (Fig. S5B). The distributions are given by Eqs. 19-21. AIC denotes Akaike information criterion based on which a better fitting distribution is chosen.

Time	Distribution	AIC	Parameter	Estimate	Std.Err.	95% CI	CV^2
4h	log-normal	-1230	σ, shape μ, log-scale	0.0812 1.38	0.000821 0.00101	(0.0796, 0.0828) (1.380, 1.384)	0.0066
	gamma	-1270	k, shape θ, scale	152 0.0263	2.93 0.000509	(146, 157) (0.0253, 0.0273)	0.0066
	Weibull	-1920	k, shape λ, scale	13.7 4.05	0.0736 0.00192	(13.6, 13.9) (4.045, 4.052)	0.0079
8h	log-normal	-1450	σ, shape μ, log-scale	0.0887 1.38	0.000744 0.000910	(0.0873, 0.0902) (1.375, 1.378)	0.0079
	gamma	-1510	k, shape θ, scale	127 0.0312	2.0 0.000494	(123, 131) (0.0303, 0.0322)	0.0079
	Weibull	-2370	k, shape λ, scale	12.4 4.03	0.0444 0.00142	(12.3, 12.5) (4.034, 4.039)	0.0096
16h	log-normal	-1690	σ, shape μ, log-scale	0.0708 1.35	0.000384 0.000470	(0.0701, 0.0716) (1.346, 1.348)	0.0050
	gamma	-1770	k, shape θ, scale	200 0.0192	2.0 0.000193	(196, 204) (0.0189, 0.0196)	0.0050
	Weibull	-1920	k, shape λ, scale	15.8 3.91	0.0715 0.00136	(15.6, 15.9) (3.905, 3.911)	0.0061

Table S4: Fitting parameters of the maximum response level, [DMOG] = 4 mM (Fig. S5C).

Time	Distribution	AIC	Parameter	Estimate	Std.Err.	95% CI	CV^2
4h	log-normal	-1590	σ, shape μ, log-scale	0.107 1.64	0.000907 0.00111	(0.105, 0.109) (1.633, 1.638)	0.011
	gamma	-1690	k, shape θ, scale	88.1 0.0584	1.36 0.000905	(85.4, 90.8) (0.0566, 0.0602)	0.011
	Weibull	-2970	k, shape λ, scale	10.6 5.27	0.0242 0.00139	(10.52, 10.62) (5.26, 5.27)	0.013
	Weibull corrected (*)	–	k, shape λ, scale	2.65 1.26	–	–	0.16
8h	log-normal	-1520	σ, shape μ, log-scale	0.109 1.71	0.00106 0.00129	(0.107, 0.111) (1.706, 1.711)	0.012
	gamma	NA	k, shape θ, scale	– –	– –	– –	– –
	Weibull	-2840	k, shape λ, scale	10.4 5.67	0.0287 0.00185	(10.3, 10.4) (5.665, 5.672)	0.014
	Weibull corrected (*)	–	k, shape λ, scale	3.37 1.70	–	–	0.11
16h	log-normal	-1130	σ, shape μ, log-scale	0.0584 1.84	0.000577 0.000706	(0.0572, 0.0595) (1.837, 1.839)	0.0034
	gamma	-1160	k, shape θ, scale	294 0.0214	5.6 0.000410	(283, 305) (0.0206, 0.0222)	0.0034
	Weibull	-2140	k, shape λ, scale	18.9 6.36	0.0727 0.00157	(18.8, 19.1) (6.361, 6.367)	0.0043
	Weibull corrected (*)	–	k, shape λ, scale	10.5 2.53	–	–	0.01

(*) R_{max} is corrected for the variability in basal level by subtracting the mean and variance of β. We use the corrected values of shape and scale parameters to sample the responses shown in Fig. 5C in the main text.

Table S5: Fitting parameters of the response threshold distribution (Fig. S5D). We fit g_{cut} distribution given by Eq. 17 to obtain parameters μ_{x50} and σ_{x50}, which are scale and shape parameters of the log-normal distribution that determines x_{50} variability.

	Results of the fitting:				Calculated stats of the x_{50} distribution:			
Time	Parameter	Estimate	Std.Err.	95% CI	Mean	Median	StDev	CV^2_{x50}
4h	σ_{x50} μ_{x50}	1.15 -0.793	0.204 0.343	(0.58, 1.71) (-1.75, 0.16)	0.87	0.45	1.44	2.72
8h	σ_{x50} μ_{x50}	0.932 -0.269	0.138 0.197	(0.55, 1.32) (-0.82, 0.28)	1.18	0.76	1.39	1.38
16h	σ_{x50} μ_{x50}	0.482 0.453	0.033 0.034	(0.39, 0.57) (0.36, 0.55)	1.77	1.57	0.90	0.26

Table S6: Evaluation of conditions 1 and 2 (Eqs. 10 & 14) using parameters calculated from experimental data: H – response steepness, σ_{x50} – shape parameter of x_{50} distribution, $m_{x50} = e^{\mu_{x50}}$ – median of x_{50} distribution, where μ_{x50} is the scale parameter of x_{50} distribution. The minimum and maximum value of DMOG limit the range of treatment for which bimodality can arise.

	Estimated from the experiment: H	shape, σ_{x50}	$m_{x50} = e^{\mu_{x50}}$	CV^2_{x50}	Condition 1: $H^2\,\sigma^2_{x50} > 2$	Condition 2: $[\text{DMOG}]_{min}$	$[\text{DMOG}]_{max}$
4h	1.56	1.15	0.45	2.72	3.22	0.32	0.64
8h	2.36	0.93	0.76	1.38	4.82	0.38	1.55
16h	3.57	0.48	1.57	0.26	2.97	1.40	1.76

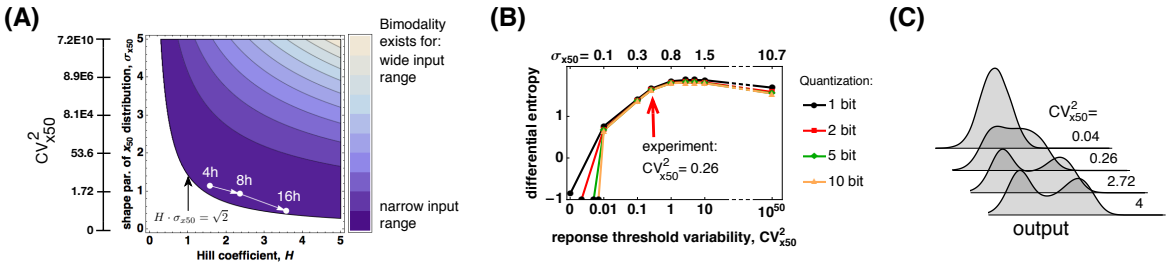

Figure S6: Numerical quantification of bimodal regime from experimental data. (A) Bimodality region as function of Hill coefficient, H, and shape parameter of the x_{50} distribution, σ_{x50}. Colour coding indicates the width of admissible input range that yields a bimodal distribution (cf. Fig. S2). Points indicate H and σ_{x50} estimated from experiments. (B) Predicted differential entropy of output distributions at 16h after treatment with $[\text{DMOG}] = 1.6nM$ (median of the threshold distribution) for a range of threshold variability. Steepness $H = 3.57$ (Table S2); β is Weibull-distributed with $k = 15.8$ and $\lambda = 3.91$ (Table S3); R_{max} is Weibull-distributed with $k = 10.5$ and $\lambda = 2.53$ (Table S4); the median of the threshold distribution $m_{x50} = 1.6$. Since the distributions are sampled numerically, Shannon entropy is calculated for decreasing histogram bin sizes (or increasing quantisations) to give the best approximation of the entropy of the continuous density. Threshold variability $CV^2_{x50} = 0.26$ ($\sigma_{x50} = 0.48$) is estimated from the experiment at 16h post-DMOG (Table S5). (C) Predicted ODD-GFP distributions for some values of CV^2_{x50} from panel B.

References

[1] S. Miller and D. Childers, *Probability and Random Processes*. With Applications to Signal Processing and Communications, Academic Press, 2012.